Biofabrication

PAPER

Aerosol jet printing of biological inks by ultrasonic delivery

Nicholas X Williams[1,4], Nathan Watson[2], Daniel Y Joh[2], Ashutosh Chilkoti[2] and Aaron D Franklin[1,3]

[1] Department of Electrical and Computer Engineering, Duke University, Durham NC 27708, United States of America
[2] Department of Biomedical Engineering, Duke University, Durham NC 27708, United States of America
[3] Department of Chemistry, Duke University, Durham NC 27708, United States of America
[4] Author to whom any correspondence should be addressed.

E-mail: nxw@duke.edu

RECEIVED
20 July 2019

REVISED
14 November 2019

ACCEPTED FOR PUBLICATION
28 November 2019

PUBLISHED
31 January 2020

Keywords: biological ink, bioprinting, aerosol jet, immunoassay

Supplementary material for this article is available online

Abstract

Printing is a promising method to reduce the cost of fabricating biomedical devices. While there have been significant advancements in direct-write printing techniques, non-contact printing of biological reagents has been almost exclusively limited to inkjet printing. Motivated by this lacuna, this work investigated aerosol jet printing (AJP) of biological reagents onto a nonfouling polymer brush to fabricate *in vitro* diagnostic (IVD) assays. The ultrasonication ink delivery process, which had previously been reported to damage DNA molecules, caused no degradation of printed proteins, allowing printing of a streptavidin-biotin binding assay with sub-nanogram ml^{-1} analytical sensitivity. Furthermore, a carcinoembryogenic antigen IVD was printed and found to have sensitivities in the clinically relevant range (limit of detection of approximately 0.5 ng ml^{-1} and a dynamic range of approximately three orders of magnitude). Finally, the multi-material printing capabilities of the aerosol jet printer were demonstrated by printing silver nanowires and streptavidin as interconnected patterns in the same print job without removal of the substrate from the printer, which will facilitate the fabrication of mixed-material devices. As cost, versatility, and ink usage become more prominent factors in the development of IVDs, this work has shown that AJP should become a more widely considered technique for fabrication.

1. Introduction

Printing has emerged as a powerful approach to simplify and reduce the cost of fabricating a broad range of devices and sensors [1–6]. This is because it enables low-cost, mask-free device production that is attractive for rapid throughput manufacturing at a fraction of the cost of competing approaches. Within the biomedical sciences, printing has shown promise in the development of *in vitro* diagnostic (IVD) assays for sensing biological analytes of interest [7, 8]. IVDs allow qualitative (yes/no) or quantitative assessment of biological analytes and play a central role in medical diagnostics [9, 10], biomedical research [11–17], and forensic science [18, 19], among other fields. While there have been many exciting demonstrations of printed IVDs, the methods for printing biological inks for these sensors are limited and could benefit from improved versatility for ease of incorporation with electrical components for the development of fully integrated electronic biosensors in the future.

To date, a mainstay approach to developing printable IVDs is inkjet printing (IJP). IJP has been used to fabricate microarrays for proteomics and genomics, as well as the widely used lateral flow immunoassay for point-of-care diagnostic testing [20–26]. In more recent work, immunoassays were fabricated using IJP to spot antibody (Ab) microarrays directly onto planar surfaces coated with a 'nonfouling' (protein- and cell-resistant) polymer film comprising poly(oligo (ethylene glycol) methacrylate) (POEGMA) brushes [27, 28]. The POEGMA brush exhibits extremely low levels of non-specific protein adsorption [29], which is typically the largest source of 'noise' in surface-based protein assays, so that assays on POEGMA can exhibit an extremely low limit of detection (LOD) [30]. The use of IJP was highly effective in embedding antibodies into the dry brush for noncovalent immobilization

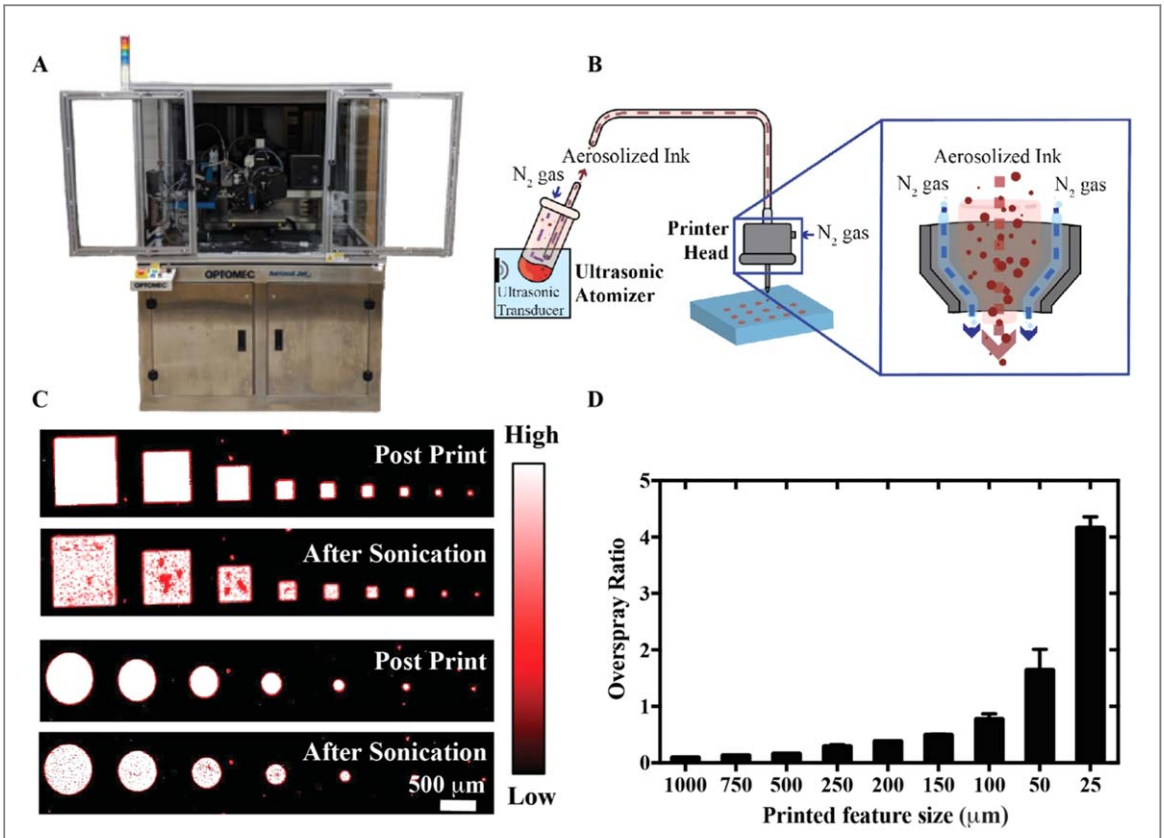

Figure 1. Aerosol jet printed biological ink. (A) Optomec Aerosol Jet 300 printer used in this work. (B) Schematic representation of ultrasonic atomization Aerosol Jet Printing (u-AJP), with a magnified view of the printer head. (C) Fluorescence images showing intensities for squares and circles of printed Cy-5 labeled BSA, captured under 647 nm light before (top) and after (bottom) sonication. (D) Overspray ratio of the aerosol jet printed shapes as a function of printed feature size.

with two additional desirable attributes. First, despite the noncovalent immobilization of antibodies, subsequent exposure of the antibodies to whiole blood, plasma or serum does not dissolve the printed antibodies. Second, embedding the antibodies into the POEGMA brush protects the antibodies from denaturation so that printed chips can be stored at room temperature for months without refrigeration.

While clearly a very useful printing technique, a major drawback to IJP is its constraint to printing inks within a narrow range of viscosities and densities. The ability to print a broader range of not only biological inks as biorecognition elements but also non-biological inks (e.g. metals, semiconductors, dielectrics, etc) as complex sensing elements is desirable as the field of printable biosensors continues to evolve.

Aerosol jet printing (AJP) is a relatively new method of printing that overcomes some of the constraints of IJP and has been used for the low-cost printing of electronics [26–30], including sensors [31–34] (figure 1(A)). AJP functions via the aerosolization of ink by ultrasonication (u-AJP) or pneumatic pressure (p-AJP). A schematic of u-AJP can be seen in figure 1(B), with a magnified view of how a sheeth of inert gas guides the aerosolized ink out of the nozzle, helping to prevent clogging. There are numerous benefits to AJP over IJP for device fabrication, including the ability to print inks with a wide range of viscosities, greater ease with printing on non-planar surfaces [35], printing high aspect ratio materials [36], and the deposition of smaller volumes [37]. Previous reports demonstrate the utility and versatility of AJP by fabricating complex transistor devices via a low-temperature printing process [38], developing a flexible pressure sensing array [33], and the creation of organic solar cells [39]. Yet, despite the considerable effort invested in applying AJP towards fabricating electronic devices, to date it has been underutilized for the deposition of biological inks, and moreover for biosensor fabrication.

Electronic devices have typically been fabricated by u-AJP rather than p-AJP. However, the limited studies available for biologics have focused on p-AJP. This is because u-AJP was presumed to be problematic for the printing of biological materials given prior evidence that the ultrasonication process denatured DNA and thus, it was postulated, denatured all larger molecules containing DNA [40]. Unfortunately, compared to ultrasonic delivery, pneumatic delivery requires a considerably greater ink volume and has a larger minimum print size. Pneumatic AJP is hence potentially problematic for production of biosensors because the most expensive elements of biological assays are typically the biorecognition elements (e.g. antibodies), where reduction of required ink volume is critical. In addition, while u-AJP may be damaging to DNA, there

is actually no empirical evidence supporting this hypothesis for other biological inks. As the vast majority of solution fabricated biosensors use antibodies or enzymes as the recognition element, investigating DNA leaves an incomplete picture and potentially limits further development. Given the limitations of the IJP process, the ability to print proteins with u-AJP could pave the way for novel platforms for low-cost proteomic and immunoassay applications that fully integrate biological and electronic components.

Motivated by these limitations of IJP and p-AJP, this study investigates the use of u-AJP to print proteins and other non-biological sensor elements. Ultrasonic AJP printing was carried out on POEGMA-coated substrates to facilitate noncovalent immobilization of protein inks and to reduce nonspecific protein adsorption on the surface. To do so, first the functionality of ultrasonically delivered streptavidin was confirmed by validating its specific binding to its ligand—biotin. Next, u-AJP was used to fabricate an immunoassay against carcinoembryogenic antigen (CEA), a clinically relevant biomarker associated with gastrointestinal malignancies that performed within the clinically relevant range for LOD. Finally, u-AJP was used to print non-biological elements (silver nanowires) during the same print job as biological elements (cy5-streptavidin). These results draw attention to u-AJP as an effective tool for multi-material printing of biological and non-biological materials on the same surface. Taken together, these findings are relevant to applications requiring controlled deposition of biological materials and for the development of next-generation IVDs requiring precise control over biological/non-biological interfaces.

2. Methods

2.1. POEGMA polymerization on glass substrates

The synthesis of the polymer brush films (POEGMA) on glass substrates is described in detail elsewhere [41]. In brief, glass substrates (Schott Nexterion Glass B; Elmsford, NY) were incubated in a 10% (v/v) 3-aminopropyltriethoxysilane (APTES) solution in ethanol (Gelest, Inc.; Morrisville, PA) overnight. After rinsing in ethanol and then water, substrate were spun dry (150 rcf) and then cured in an oven for approximately 2 h at 120 °C and then stored at room temperature. Next, substrates were placed in a dichloromethane (DCM) solution containing 1% trimethylamine and 1% alpha-bromoisobutyryl bromide (Sigma-Aldrich; St. Louis, MO) for 30 min under continuous stirring. Chips were cleaned by serial rinses in fresh DCM, ethanol, and then water. A polymerization solution was next prepared by adding 30 mg of copper(II) bromide, 50 μl of 1,1,4,7,10,10-Hexamethyltriethylenetetramine (HMTETA), and 75 g of poly(ethylene glycol) methyl ether methacrylate monomer (MW ~ 300 Da) to 350 ml of water. This solution degassed by gently sparging under helium for 3 h. Finally, 650 mg of sodium ascorbate was added to this degassed solution under an Argon environment and samples were immersed for 4 h in this polymerization solution. Substrates were then rinsed thoroughly in water, centrifuged dry, and then stored at room temperature. Thickness of polymer brush layers were characterized utilizing a M-88 spectroscopic reflective mode ellipsometer (J.A. Woollam Co; Lincoln, NE). Measurements were obtained at 65°, 70°, and 75° at wavelengths between 400 and 800 nm and fit utilizing a Cauchy model.

2.2. Biological ink printing

AJP was performed on an AJ-300 printer (Optomec; Albuquerque, NM) equipped with a 100 μm nozzle. Unless otherwise noted, all inks were prepared at 0.20 mg ml^{-1} suspended in phosphate buffered serum (PBS). The printer was set with sheath gas, atomizer, and ultrasonic current of approximately 16 standard cubic centimeters per minute (SCCM), 16 SCCM, and 320 mA, respectively. Printing speed was maintained at 0.5 mm s^{-1} with a fixed platen temperature of 30 °C to facilitate ink drying. All printing was performed under ambient room conditions. Cy5 conjugated bovine serum albumin (BSA) (ThermoFisher Scientific, Waltham MA), streptavidin (Thermo Fischer Scientific; Waltham, MA), and anti-cancer embryogenic antigen antibody (anti-CEA) (Roche Holding AG; Basel, Switzerland) inks were printed by AJP. IJ printing was performed utilizing a non-contact sciFLEXARRAYER S11 printer (Scienion, Inc.; Berlin, Germany). Printing was performed in a cleanroom setting with the same inks used for AJ printing.

2.3. Fluorescent imaging

Fluorescence imaging of Cy5 and Alexa Fluor 488 labels was performed with an Axon Genepix 4400 tabletop scanner (Molecular Devices, LLC; San Jose, CA). Spot intensities were measured and analyzed by ImageJ Fiji. Data were plotted with Graphpad Prism (Graphpad Software Inc.; La Jolla, CA).

2.4. Protein adhesion and overspray calculation

POEGMA-coated substrates with spots of printed Cy5-BSA were serially washed and sonicated (Crest Ultrasonics CP230D—Peak power 160 W with an average power of 80 W) in deionized water to assess protein surface immobilization. Extent of protein retention following each treatment was assessed via fluorescent imaging of chips compared to baseline intensities. Overspray area was assessed and compared to printed area to calculate an overspray ratio (OR), defined as OR = (Areaoverspray/Areafeature) [42]. Overspray and feature areas were determined via ImageJ Fiji software with pixel distance fixed at 2.5 μm.

2.5. Streptavidin-biotin binding studies

Cy5-streptavidin (ThermoFisher Scientific, Waltham, MA) was printed by u-AJP or IJP onto POEGMA-coated glass samples. Following printing, substrates were gently cured at 30 °C overnight to facilitate spot drying. Printed arrays were exposed to a dilution series of Alexa Fluor 488-labeled biotin spiked in fetal bovine serum (FBS) and incubated under gentle orbital agitation for 1 h. Following incubation, chips were rinsed in 0.1% Tween-20/PBS wash buffer and subsequently spun dry with a slide centrifuge (Labnet, Edison, NJ) for 15 s.

2.6. Sandwich immunoassays

Anti-CEA immunoassays were fabricated by either AJ or IJ printing onto POEGMA-coated glass substrates. Anti-CEA capture and detection antibody pairs were selected according to the manufacturer's guidelines (Roche Holding AG; Basel, Switzerland). Immunoassays were incubated with a dilution series of spiked CEA antigen (BiosPacific, Inc.; Emeryville, CA) in FBS for 1 h on continuous orbital rotation. Following incubation, the arrays were briefly washed in 0.1% (v/v)Tween-20/PBS wash buffer and spun dry. Next, chips were incubated with 100 μl of 5 μg ml^{-1} Cy5-labeled detection antibody (dAB) in PBS with BSA (1% (w/v)) for 1 h under similar orbital agitation. Antibody-fluorophore conjugation was performed utilizing an Alexa Fluor 647 antibody labeling kit (Molecular Probes; Eugene, OR). Following incubation, chips were washed one more time utilizing the same methods as before.

2.7. Silver nanowire ink printing

Silver nanowire inks were synthesized using the polyol process reported in [43]. Briefly, 160 ml of ethylene glycol (EG) (J.T. Baker, USA) was heated to 150 °C in a round-bottom flask for 1 h. Four solutions were then made: (1) 0.257 g NaCl (Fischer Scientific) in 20 ml EG, (2) 0.08 g of $Fe(NO_3)_3$ (Sigma Aldrich, USA), (3) 1.05 g polyvinylpyrrolidone in 25 ml EG, and (4) 1.05 g silver nitrate (Fischer Scientific, USA) in 25 ml EG. Next, 0.2 ml of solution 1, 0.1 ml of solution 2, 20.76 ml of solution 3, and 20.76 ml of solution 4 were added in 30 s increments to the preheated 500 ml flask. The solution was stirred at 250 RPM for 1 h. After the synthesis, the silver nanowires were washed twice in acetone (VWR, USA) and once in deionized water. The silver nanowires were then suspended in water at a concentration of 10 mg ml^{-1} and 0.1% v/v hydroxypropyl methylcellulose was added to enhance the viscosity and surface tension of the ink. The silver nanowire ink was printed using an AJ printer with an ultrasonic current of 350 mA, an atomizer flow of 35 SCCM, and a sheath flow of 25 SCCM. A 200 μm nozzle was selected, and the printed platen was set at 30 °C to match the temperature at which the biological ink were printed.

2.8. Scanning electron microscopy (SEM)

SEM was performed using an Apreo S (ThermoFisher Scientific, USA). An accelerating voltage of 2 kV and an emission current of 25 pA was used. To reduce charging effects, samples were electrically grounded with copper tape.

3. Results

3.1. AJ printing feasibility and resolution

The ability of u-AJP to deposit biological inks onto POEGMA-coated planar surfaces was first characterized by using fluorescence imaging of printed Cy5-labeled BSA (Cy5-BSA) as a model protein. We investigated the well-known tendency in AJP for small droplets of ink to deviate from the intended print line (known as 'overspray'), caused by errant aerosolized droplets that are not fully contained by the sheath flow, which can adversely affect printer resolution. To evaluate the overspray of Cy5-BSA by u-AJP, squares and circles of sequentially smaller sizes were printed onto a POEGMA surface as shown in figure 1(C). Both the square and circular features retained sharp feature definition at side lengths down to 100 μm, while the edges of the squares began to lose definition below the 100 μm limit. To quantitate printer overspray, a so-called 'overspray ratio' for circles was calculated by dividing the area enclosed in the overspray by the area of the printed shape, OR = ($\text{Area}_{\text{overspray}}/\text{Area}_{\text{feature}}$), adapted from [44]. As shown in figure 1(D), for large printed sizes (>500 μm) the overspray was negligible in comparison to the size of the printed shape; however, as the printed surface area decreased, the overspray ratio increased in an inverse power relationship. At a resolution below 50 μm, the overspray area is of similar size to the print itself, leading to reduced fidelity in printed features. To avoid the possibility of bridging the small gap with overspray deposition, a small gap of at least 20 μm between printed features is hence necessary.

However, for prints with a larger spacing between features (e.g. IVDs), large separation with almost no overspray between printed spots can be observed. As seen in the high magnification image and intensity profile of figure S1 which is available online at stacks.iop.org/BF/12/025004/mmedia, fluorescence intensity decreases over a small distance outside the intended printed area for a 20 μm spot size, with almost no fluorescence observed at a distance of 10 μm from the intended print. This overspray area contributes a minimal fluorescence intensity and contributes to <20% of the overall fluorescence intensity, suggesting that a minimal volume of ink is lost to overspray. Although overspray results in lower fidelity for printing small, complex structures with a line spacing of less than 20 μm, protein microarrays or IVDs typically utilize feature sizes >50 μm [45–48], and in this size regime the overspray intrinsic to AJP should not

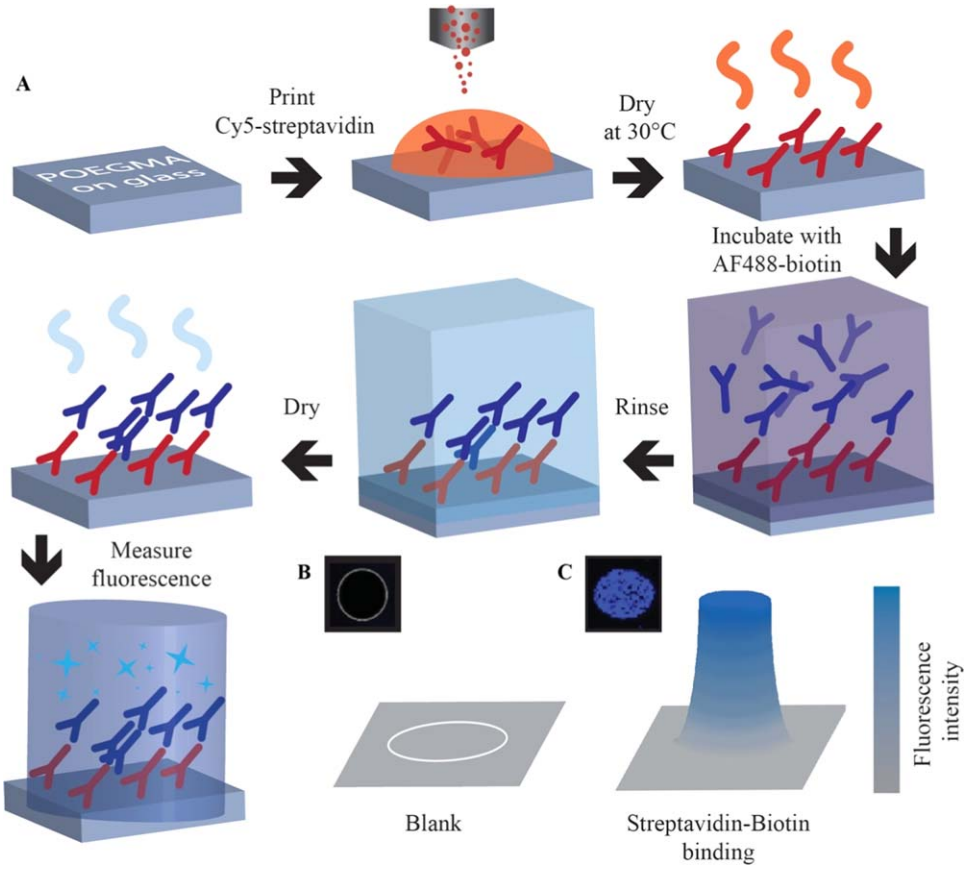

Figure 2. Approach to IVD fabrication and testing. (A) Schematic process flow: Cy5-streptavidin printed onto POEGMA-coated glass slides using u-AJP. Deposition dried overnight at 30 °C, then incubated in a dilution series of AF488-biotin and rinsed in 0.1% Tween-20/PBS then dried by centrifugation for 10 s. Binding event of AF488-biotin to Cy5-streptavidin is characterized by fluorescence. A representative florescent image and cartoon of the fluorescent intensity from a printed feature that is blank (B) and one with significant binding events (C).

negatively affect the performance of the printed assay. Additionally, the utilization of an appropriate printing surface that is well-suited for noncovalent immobilization of printed proteins with minimal background noise is pivotal [28]. As highlighted in figure S2, at a high enough ink concentration (0.2 mg ml^{-1}) POEGMA-coated surfaces retain reagents delivered by u-AJP as demonstrated with maintained fluorescence after increasingly energetic rinsing steps.

3.2. Binding of biotin to ultrasonically deposited streptavidin

The ability of u-AJP to be used for microarray and IVD applications was next investigated. To test retention of protein function after u-AJP printing, streptavidin was selected as a model protein because it has a high affinity for biotin—a small molecule ligand—only in its folded state, and the ability of streptavidin to bind biotin is hence a good test of the retention of protein structure and function after u-AJP printing. As shown in figure 2, spots of Cy5-streptavidin were printed by u-AJP at a concentration of 0.2 mg ml^{-1} onto POEGMA-coated glass to serve as surface-immobilized capture reagents. These samples were then exposed to a dilution series of Alexa Fluor 488-tagged biotin (AF488-biotin) to generate dose-response curves to analyse assay performance.

A representative fluorescence image of Cy5-streptavidin capture spots printed by u-AJP is shown in figure 3(A) (red channel), along with the fluorescence response of these spots following incubation with either: (1) PBS spiked with AF488-biotin or (2) PBS (blue channel). The binding of AF488-biotin localized to capture spots in samples fabricated by u-AJP suggests preservation of streptavidin bioactivity under the ultrasonication settings used here. Outside the capture spots, very low background fluorescence levels are observed, which is consistent with the lack of nonspecific binding AF488-biotin to the surface (figure S3). Full dose-response curves for u-AJP are shown in figure 3(B) and demonstrate a LOD of 0.22 ng ml^{-1} for biotin-streptavidin binding and a dynamic range (DR) of more than 3 orders of magnitude.

Given the importance of the minimization of ink usage, the effect of spot sizes on dose-response parameters were next investigated. As can be observed

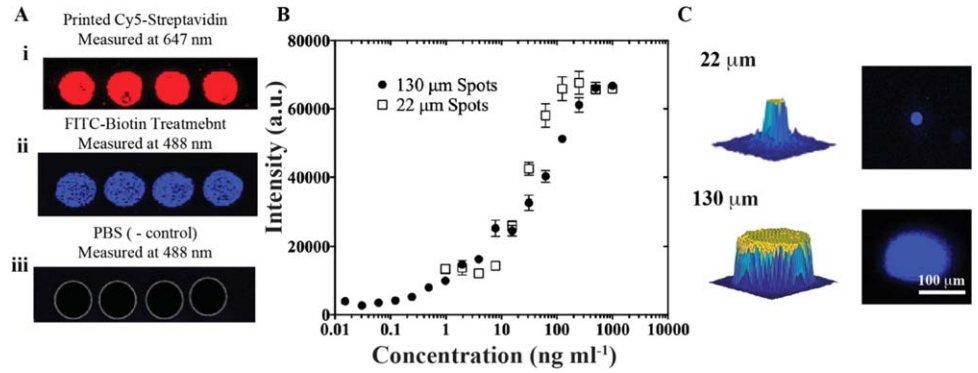

Figure 3. Confirmation of preserved biofunctionality following u-AJP printing and comparison of large and small spot sizes using streptavidin-biotin assay. (A) i. Printed spots of Cy5-streptavidin measured at 647 nm, then similar spots observed at 488 nm after: ii. Treatment with FITC-conjugated biotin showing active binding, and iii. Rinsing with PBS control without any biotin incubation. (B) Dose-response curve from AJP-printed assay of streptavidin-biotin. Data represent average ± SD of 3 separately run assays. (C) 3D (left) and 2D (right) images of FITC-biotin-treated single spots from the AJP with a 22 μm (top) and 130 μm diameter (bottom), imaged at 488 nm.

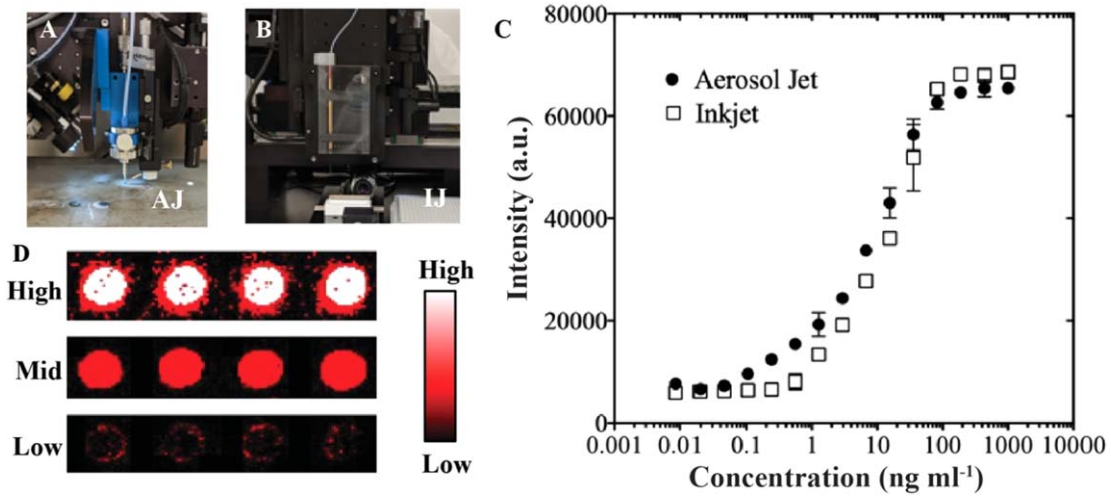

Figure 4. Printed anti-CEA immunoassay comparing u-AJP to IJP. Photographs of (A) optomec aerosol jet printer head and (B) Scienion inkjet printer head. (C) Dose-response curves from u-AJ and IJ printed anti-CEA assays with a spot size of ~130 μm. Data represent average ± SD of 3 separately run assays. (D) Characteristic fluorescence response of printed anti-CEA capture antibody against spiked CEA antigen concentration at high (top), middle (mid), and low (bottom) CEA concentrations.

from the representative 2D and 3D profiles of spots in figure 3(C), the minimum achievable spot diameter with a 100 μm nozzle for u-AJP was 22 μm, whereas the baseline spot has a diameter of 130 μm. This droplet miniaturization corresponds to a significant 35-fold decrease in aerosolized volume, which would lead to a dramatic reduction in antibody usage and hence cost. An image of a printed streptavidin array at multiple levels of magnification can be seen in figure S4. The spots have a uniform profile without considerable fluorescence intensity outside of the intended spot area. Under these conditions, the dose-response curve for the 22 μm spots exhibit a LOD of 12.2 ng ml^{-1}, an ~1.5 log DR from ~10 to 400 ng ml^{-1} (figure 3(B)) and an identical maximum fluorescence intensity at the highest biotin-AF488 concentrations as the larger spot with a diameter of 130 μm.

3.3. Sandwich immunoassay against CEA via u-AJP of Ab microarrays

Next, the functionality of u-AJP compared to IJP was investigated via the fabrication of antibody-based microarrays to detect carcinoembryonic antigen (CEA), a clinically relevant serum tumor marker commonly associated with gastrointestinal malignancies [49]. CEA has a diagnostic cut-off ranging from ~5 to 20 ng ml^{-1}, and these values are typically measured in the clinical laboratory by enzyme linked immunosorbent assay (ELISA). For these experiments, microspots of anti-CEA capture antibodies were printed by either u-AJP (figure 4(A)) or IJP (figure 4(B)), both with spot sizes of ~130 μm. The assay fabrication process flow is illustrated in figure S5. Ab microarrays were exposed to undiluted calf serum spiked with varying amounts of CEA, washed, and then labeled with an anti-CEA detection Ab. The data

show that immunoassays fabricated by IJP and u-AJP (figure 4(C)) had similar LODs and DRs, with a LOD in the sub-nanogram ml^{-1} range (552 pg ml^{-1} and 412 pg ml^{-1}, respectively), and with a DR of ~3 orders of magnitude. Representative fluorescence images of high, medium, and low concentrations of CEA antigen are shown in figure 4(D). These results show that antibodies deposited by u-AJP maintained binding functionality with similar sensitivities and overall performance as antibodies deposited by IJP.

3.4. Mixed-material printing

Ultrasonic AJP has been used extensively for the deposition of materials for electrical devices [33, 50–52]. Having shown that u-AJP also enables printing of biological inks, the flexibility of u-AJP to print complex structures comprised of both biological reagents and electrically conductive materials in an integrated manner was next investigated. This has the potential to reduce the logistical burden and overhead cost of next-generation electronic biosensor fabrication due to the reduction of required sample transfer from one fabrication process to another. u-AJP is uniquely suited for this in-place biosensor printing due to its ability to print complex structures without removal of the sample from the printer platen [38] as well as its ability to print conductive traces at room temperature [36].

To demonstrate the printing of multi-material structures, the logo of the Duke University Chapel was printed with both silver nanowires and Cy5-streptavidin (figures 5(A), (B)). The windows of the chapel were first printed with Cy5-streptavidin; then, without removal of the substrate from the printer platen, conductive traces were printed at room temperature from high aspect ratio silver nanowires, a material known to be challenging to print by IJP due to clogging issues [53]. The fluorescent image in figure 5(B) shows the distinct boundary between the Cy5-streptavidin regions and the conductive nanowires.

A higher resolution analysis of the interface between the streptavidin and nanowires was carried out by SEM (figures 5(C), (E)). The order of the print process has an impact on the definition of these boundaries, as seen in the fluorescence image in figure S6 where the inks were printed in reverse order. When printed after the silver nanowires, the biological ink diffuses into the nanowire region, increasing the fluorescence area and decreasing the stark printing boundary distinction. This is either due to capillary action or diffusion of compatible solvents between the nanowires and streptavidin.

4. Discussion

The ability of AJP to print a broader range of ink viscosities and nanoscale morphologies than IJP has been explored in this work. To date, AJP has almost exclusively been used for the development of electrically conductive films and devices with some distinct advancements in the versatility of the print process. These include recent reports that AJP enables the printing of inks composed of relatively large, conductive nanostructures at room temperature [36], and the use of AJP to print functional electronic devices without removing the substrate from the printer [38]. The realization of printing proteins with AJP in this work further expands its capabilities and opens the way for more complex devices that integrate biological and non-biological elements to be realized. Since prior work demonstrateed that u-AJP induces damage to DNA [40], our finding that the use of ultrasonic energy in u-AJP does not denature the biofunctionality of proteins is a significant advancement, especially considering the previously held assumption that an ultrasonic process is generally incompatible with biological reagents. Hence, this discovery opens a new avenue for biosensor fabrication, allowing for the deposition of a broad range of biological inks with u-AJP.

As demonstrated herein, u-AJP enables the rapid and simple fabrication of IVD assays with sub-ng ml^{-1} LOD. These results will likely extend to any analyte for which an established Ab pair is available. The LOD is well within the clinically relevant concentrations for various biomarkers, including prostate specific antigen [54], creatine-kinase muscle/brain [55], and leptin [56]. This indicates that the deposition of biomarkers with u-AJP onto POEGMA-coated surfaces could be broadly applicable as a general platform for highly sensitive IVD assays.

Given the high cost associated with antibodies, there is a desire to decrease the total printed volume while maintaining the sensitivity of an IVD assay [57]. One significant drawback of AJP is the high volume of ink required for printing with the ultrasonic atomizer (500–1000 μl) as compared to the volume required to fill an IJP well (as low as 10 μl). This potentially could limit the development of IVD assays with an AJ printer; however, given the relatively low levels of damage associated with the ultrasonication, there is strong evidence that the ink in the atomizer can be retained for further use, decreasing the waste associated with the printing process. In addition, this issue will decrease in relevance as this process is scaled up.

In tandem, reduction of the printed volume is desirable for fabrication of low-cost biosensors. This work demonstrates the ability to fabricate an IVD assay via u-AJP with minimal printed biological ink volume; although, the LOD did increase from sub-ng ml^{-1} to 10 ng ml^{-1} with a decreased DR. Hence, for scaled production of assays, print volumes can likely be adjusted to balance the required sensitivity (depending on the application) versus the amount of protein ink that is consumed. For highly sensitive assays, larger spot size may be required in order to

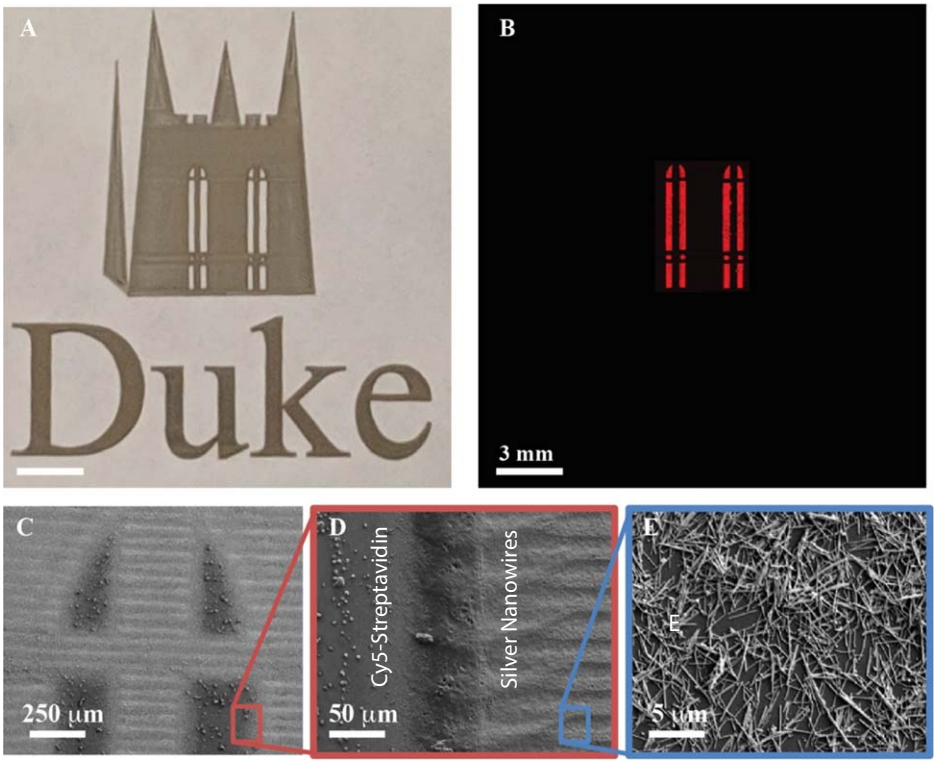

Figure 5. Mixed-material ultrasonic aerosol jet printing. (A) Optical photograph of the Duke Chapel and 'Duke' printed with silver nanowires, and the windows printed with Cy5-streptavidin. (B) Fluorescence image (measured at 647 nm) of same print area showing the localized regions of printed biological ink. SEM images of (C) the window region of the print and higher magnification views of (D) the interface between the silver nanowires and streptavidin and (E) the silver nanowires.

maintain the sub-nanogram sensitivity; however, with cancer markers (such as CEA) where the diseased state presents with an elevated marker concentration, highly sensitive assays are not required. Future research on the reduction of printed ink volume should explore this relationship further to optimize the droplet volume for a total reduction in ink usage while maintaining a sufficiently low LOD.

In addition to fabricating IVD assays with minimal Ab ink usage, AJP also allows printing of more complex devices and structures. The ability for multi-material printing that is facilitated by the ultrasonication and protective sheath flow intrinsic to u-AJP enables the deposition of a wide variety of materials. The demonstration of printing electrically conductive silver nanowires with biologically active Cy5-streptavidin in a single, print-in-place process is evidence of this multi-material printing capability. With the growing interest in realizing IVD assays with electrically transduced detection of binding events, [58–64] having a printing approach for both electrical and biological inks is a significant boon.

5. Conclusion

The ability to use u-AJP to print functional biological reagents into arbitrary and scalable shapes has been demonstrated. While previous studies suggested that ultrasonication may be damaging to biomolecules, based on DNA damage from u-AJP, no indication of damage to protein reagents was observed. Highly sensitive immunoassays were printed via the ultrasonic atomization mode of an aerosol jet printer onto POEGMA-coated substrates, showing that the printed biological inks retained their biofunctionality. These biosensors exhibited sensitivities in the pg ml^{-1} range, which was consistent with comparable biosensors printed with an inkjet printer—further evidence that the u-AJP process is compatible with protein inks. Finally, to demonstrate the flexibility of u-AJP, both conductive traces as well as biological materials were printed on the same printer without removal of the substrate from the platen. As cost, throughput, versatility, and ink usage become more prominent factors in the development of IVD assays, AJP should become a more widely considered technique for fabrication of devices that integrate biological and non-biological elements.

Acknowledgments

This work was supported by the Department of Defense Congressionally Directed Medical Research Program (CDMRP) under award number W81XWH-17-2-0045 and by the National Institutes of Health (NIH) under award number 1R21HL141028.

ORCID iDs

Nicholas X Williams https://orcid.org/0000-0003-0783-9573
Aaron D Franklin https://orcid.org/0000-0002-1128-9327

References

[1] Hu G *et al* 2017 Black phosphorus ink formulation for inkjet printing of optoelectronics and photonics *Nat. Commun.* **8** 278
[2] Cao C, Andrews J B and Franklin A D 2017 Completely printed, flexible, stable, and hysteresis-free carbon nanotube thin-film transistors via aerosol jet printing *Adv. Electron. Mater.* **3** 1–10
[3] Mohammed M G and Kramer R 2017 All-printed flexible and stretchable electronics *Adv. Mater.* **29** 1604965
[4] Scheideler W J, McPhail M, Kumar R, Smith J and Subramanian V 2018 Scalable, high-performance printed InO_x transistors enabled by UV-annealed printed high-k AlO_x gate dielectrics *ACS Appl. Mater. Interfaces* **10** 37277–86
[5] Karim N, Afroj S, Malandraki A, Butterworth S, Beach C, Rigout M, Novoselov K, Casson A J and Yeates S 2017 All inkjet-printed graphene-based conductive pattern for wearable e-textiles application *J. Mater. Chem.* C **5** 11640–8
[6] Hondred J A, Breger J C, Alves N J, Trammell S A, Walper S A, Medintz I L and Claussen J C 2018 Printed graphene electrochemical biosensors fabricated by inkjet maskless lithography for rapid and sensitive detection of organophosphates *ACS Appl. Mater. Interfaces* **10** 11125–34
[7] Glavan A C, Niu J, Chen Z, Güder F, Cheng C M, Liu D and Whitesides G M 2016 Analytical devices based on direct synthesis of DNA on paper *Anal. Chem.* **88** 725–31
[8] Yu X Y 2016 *Advances in Microfluidics: New Applications in Biology, Energy, and Materials Sciences* (London: Intech)
[9] A Albini, Y Iwamoto and H K Kleinman 1987 A rapid *in vitro* assay for quantitating the invasive potential of tumor cells *Cancer Res.* **47** 3239–45
[10] Hartmann A, Sasaki Y F, Tice R R, Rojas E, Anderson D, Miyamae Y, Agurell E, Burlinson B, Ryu J-C and Kobayashi H 2002 Single cell gel/comet assay: Guidelines for *in vitro* and *in vivo* genetic toxicology testing *Environ. Mol. Mutagen.* **35** 206–21
[11] Polli J W, Wring S A and Humphreys J E 2001 Rational use of *in vitro* P-glycoprotein assays in drug discovery *J. Pharmacol. Exp. Ther.* **299** 620–8
[12] Chang R, Emami K, Wu H and Sun W 2010 Biofabrication of a three-dimensional liver micro-organ as an *in vitro* drug metabolism model *Biofabrication* **2** 45004
[13] Scudiero D, McMahon J, Vistica D, Storeng R, Skehan P, Warren J T, Kenney S, Monks A, Boyd M R and Bokesch H 2007 New colorimetric cytotoxicity assay for anticancer-drug screening *JNCI J. Natl. Cancer Inst.* **82** 1107–12
[14] Wienkers L C and Heath T G 2005 Predicting *in vivo* drug interactions from *in vitro* drug discovery data *Nat. Rev. Drug Discovery* **4** 825–33
[15] Jones C F and Grainger D W 2009 *In vitro* assessments of nanomaterial toxicity *Adv. Drug Deliv. Rev.* **61** 438–56
[16] Diekjürgen D and Grainger D W 2018 Drug transporter expression profiling in a three-dimensional kidney proximal tubule *in vitro* nephrotoxicity model *Pflugers Arch. Eur. J. Physiol.* **470** 1311–23
[17] Chen J *et al* 2019 Glycan targeted polymeric antibiotic prodrugs for alveolar macrophage infections *Biomaterials* **195** 38–50
[18] Cooper G A A, Kronstrand R and Kintz P 2012 Society of hair testing guidelines for drug testing in hair *Forensic Sci. Int.* **218** 20–4
[19] Frumkin D, Wasserstrom A, Davidson A and Grafit A 2010 Authentication of forensic DNA samples *Forensic Sci. Int. Genet.* **4** 95–103
[20] Barbulovic-Nad I, Lucente M, Sun Y, Zhang M, Wheeler A R and Bussmann M 2006 Bio-microarray fabrication techniques—a review *Crit. Rev. Biotechnol.* **26** 237–59
[21] Calvert P 2001 Inkjet printing for materials and devices *Chem. Mater.* **13** 3299–305
[22] Dufva M 2005 Fabrication of high quality microarrays *Biomol. Eng.* **22** 173–84
[23] Pelton R, Su S, Ali M, Filipe C D M and Li Y 2008 Microgel-based inks for paper-supported biosensing applications *Biomacromolecules* **9** 935–41
[24] Walcarius A, Minteer S D, Wang J, Lin Y and Merkoçi A 2013 Nanomaterials for bio-functionalized electrodes: recent trends *J. Mater. Chem.* B **1** 4878–908
[25] Bracher P J, Gupta M and Whitesides G M 2010 Patterning precipitates of reactions in paper *J. Mater. Chem.* **20** 5117–22
[26] Sajid M, Kawde A N and Daud M 2015 Designs, formats and applications of lateral flow assay: a literature review *J. Saudi Chem. Soc.* **19** 689–705
[27] Joh D Y *et al* 2017 Inkjet-printed point-of-care immunoassay on a nanoscale polymer brush enables subpicomolar detection of analytes in blood *Proc. Natl Acad. Sci.* **114** 7054–62
[28] Hucknall A *et al* 2009 Simple fabrication of antibody microarrays on nonfouling polymer brushes with femtomolar sensitivity for protein analytes in serum and blood *Adv. Mater.* **21** 1968–71
[29] Ma H, Hyun J, Stiller P and Chilkoti A 2004 'Non-fouling' oligo(ethylene glycol)-functionalized polymer brushes synthesized by surface-initiated atom transfer radical polymerization *Adv. Mater.* **16** 338–41
[30] Hucknall A, Rangarajan S and Chilkoti A 2009 In pursuit of zero: polymer brushes that resist the adsorption of proteins *Adv. Mater.* **21** 2441–6
[31] Liu R, Ding H, Lin J, Shen F, Cui Z and Zhang T 2012 Fabrication of platinum-decorated single-walled carbon nanotube based hydrogen sensors by aerosol jet printing *Nanotechnology* **23** 505301
[32] Andrews J B, Cao C, Brooke M A and Franklin A D 2017 Noninvasive material thickness detection by aerosol jet printed sensors enhanced through metallic carbon nanotube ink *IEEE Sens. J.* **17** 4612–8
[33] Andrews J B, Cardenas J A, Lim C J, Noyce S G, Mullett J and Franklin A D 2018 Fully printed and flexible carbon nanotube transistors for pressure sensing in automobile tires *IEEE Sens. J.* **18** 7875–80
[34] White S P, Frisbie C D and Dorfman K D 2018 Detection and sourcing of gluten in grain with multiple floating-gate transistor biosensors *ACS Sensors* **3** 395–402
[35] Wilkinson N J, Smith M A A, Kay R W and Harris R A 2019 A review of aerosol jet printing—a non-traditional hybrid process for micro-manufacturing *Int. J. Adv. Manuf. Technol.* **105** 4599–619
[36] Williams N X, Noyce S G, Cardenas J A, Catenacci M J, Wiley B J and Franklin A D 2019 Silver nanowire inks for room temperature electronic tattoo applications *Nanoscale* **11** 14294-14302
[37] Cai F, Pavlidis S, Papapolymerou J, Chang Y H, Wang K, Zhang C and Wang B 2014 Aerosol jet printing for 3D multilayer passive microwave circuitry *2014 44th European Microwave Conference* (Rome) pp 512–5
[38] Cardenas J A, Catenacci M J, Andrews J B, Williams N X, Wiley B J and Franklin A D 2018 In-place printing of carbon nanotube transistors at low temperature *ACS Appl. Nano Mater.* **1** 1863–9
[39] Yang C, Zhou E, Miyanishi S, Hashimoto K and Tajima K 2011 Preparation of active layers in polymer solar cells by aerosol jet printing *ACS Appl. Mater. Interfaces* **3** 4053–8
[40] Grunwald I, Groth E, Wirth I, Schumacher J, Maiwald M, Zoellmer V and Busse M 2010 Surface biofunctionalization and production of miniaturized sensor structures using aerosol printing technologies *Biofabrication* **2** 14106
[41] Yager P, Domingo G J and Gerdes J 2008 Point-of-care diagnostics for global health *Ann. Rev. Biomed. Eng.* **10** 107–44

[42] Seifert T, Sowade E, Roscher F, Wiemer M, Gessner T and Baumann R R 2015 Additive manufacturing technologies compared: morphology of deposits of silver ink using inkjet and aerosol jet printing *Ind. Eng. Chem. Res.* **54** 769–79
[43] Stewart I E, Kim M J and Wiley B J 2017 Effect of morphology on the electrical resistivity of silver nanostructure films *ACS Appl. Mater. Interfaces* **9** 1870–6
[44] Salary R, (Ross), Lombardi J P, Samie Tootooni M, Donovan R, Rao P K, Borgesen P and Poliks M D 2016 Computational fluid dynamics modeling and online monitoring of aerosol jet printing process *J. Manuf. Sci. Eng.* **139** 021015
[45] Hu Z, Zhang A, Storz G, Gottesman S and Leppla S H 2006 An antibody-based microarray assay for small RNA detection *Nucleic Acids Res.* **34** 1–7
[46] Ekins R P and Chu F W 1991 Multianalyte microspot immunoassay—microanalytical 'compact disk' of the future *Clin. Chem.* **31** 1955–67
[47] Joos T O *et al* 2000 A microarray enzyme-linked immunosorbent assay for autoimmune diagnostics *Electrophoresis* **21** 2641–50
[48] Sergeev N, Volokhov D, Chizhikov V and Rasooly A 2004 Simultaneous analysis of multiple staphylococcal enterotoxin genes by an oligonucleotide microarray assay *J. Clin. Microbiol.* **42** 2134–43
[49] Moertel C G, Fleming T R, Macdonald J S, Haller D G, Laurie J A and Tangen C 1993 An evaluation of the carcinoembryonic antigen (CEA) test for monitoring patients with resected colon cancer *JAMA J. Am. Med. Assoc.* **270** 943–7
[50] Cardenas J A, Upshaw S, Williams N X, Catenacci M J, Wiley B J and Franklin A D 2019 Impact of morphology on printed contact performance in carbon nanotube thin-film transistors *Adv. Funct. Mater.* **29** 1–7
[51] Jones C S, Lu X, Renn M, Stroder M and Shih W S 2010 Aerosol-jet-printed, high-speed, flexible thin-film transistor made using single-walled carbon nanotube solution *Microelectron. Eng.* **87** 434–7
[52] Jabari E and Toyserkani E 2015 Micro-scale aerosol-jet printing of graphene interconnects *Carbon* **91** 321–9
[53] Finn D J, Lotya M and Coleman J N 2015 Inkjet printing of silver nanowire networks *ACS Appl. Mater. Interfaces* **7** 9254–61
[54] Lilja H, Ulmert D and Vickers A J 2008 Prostate-specific antigen and prostate cancer: prediction, detection and monitoring *Nature Reviews Cancer* **8** 268–78
[55] Puelo P R *et al* 2006 Use of a rapid assay of subforms of creatine kinase MB to diagnose or rule out acute myocardial infarction *Surv. Anesthesiol.* **39** 40
[56] Bartz S *et al* 2014 Severe acute malnutrition in childhood: hormonal and metabolic status at presentation, response to treatment, and predictors of mortality *J. Clin. Endocrinol. Metab.* **99** 2128–37
[57] Barron J A, Young H D, Dlott D D, Darfler M M, Krizman D B and Ringeisen B R 2005 Printing of protein microarrays via a capillary-free fluid *Proteomics* **6** 4138–44
[58] Guo C, Li H, Zhang X, Huo H and Xu C 2015 3D porous CNT/MnO_2 composite electrode for high-performance enzymeless glucose detection and supercapacitor application *Sensors Actuators* B **206** 407–14
[59] Tian B and Lieber C M 2019 Nanowired bioelectric interfaces *Chem. Rev.* **119** 9136–52
[60] Pavinatto F J, Paschoal C W A and Arias A C 2015 Printed and flexible biosensor for antioxidants using interdigitated ink-jetted electrodes and gravure-deposited active layer *Biosens. Bioelectron.* **67** 553–9
[61] Nguyen T, Lam S, Park H, Shi R and Lee H 2018 Development of flexible glutamate biosensor using activated carbon—Pt microparticle composite ink *IEEE Sens.* **2018** 1–4
[62] Vargas A E, Teymourian H, Tehrani F, Eksin E, Sánchez-tirado E, Warren P, Erdem A and Wang J 2019 Enzymatic/immunoassay dual biomarker sensing chip: towards decentralized insulin/glucose detection *Angew. Chemie Int. Ed.* **58** 6376
[63] Hajian R *et al* 2019 Detection of unamplified target genes via CRISPR–Cas9 immobilized on a graphene field-effect transistor *Nat. Biomed. Eng.* **3** 427–37
[64] White S P, Sreevatsan S, Frisbie C D and Dorfman K D 2016 Rapid, selective, label-free aptameric capture and detection of ricin in potable liquids using a printed floating gate transistor *ACS Sensors* **1** 1213–6